J. Membrane Biol. 165, 19–35 (1998)

The Journal of
Membrane
Biology

How Powerful is the Dwell-Time Analysis of Multichannel Records?

R. Blunck, U. Kirst, T. Riessner, U.-P. Hansen
Institute of Applied Physics, University of Kiel, 24098 Kiel, Germany

Received: 9 June 1997/Revised: 28 April 1998

Abstract. Exact algorithms for the kinetic analysis of multichannel patch-clamp records require hours to days for a single record. Thus, it may be reasonable to use a fast but less accurate method for the analysis of all data sets and to use the results for a reanalysis of some selected records with more sophisticated approaches. For the first run, the tools of single-channel analysis were used for the evaluation of the single-channel rate constants from multichannel dwell-time histograms. This could be achieved by presenting an ensemble of single channels by a ''macrochannel'' comprising all possible states of the ensemble of channels. Equations for the calculations of the elements of the macrochannel transition matrix and for the steady-state concentrations for individual states are given. Simulations of multichannel records with 1 to 8 channels with two closed and one open states and with 2 channels with two open and two closed states were done in order to investigate under which conditions the one-dimensional dwell-time analysis itself already provides reliable results. Distributions of the evaluated single-channel rate constants show that a bias of the estimations of the single-channel rate constants of 10 to 20% has to be accepted. The comparison of simulations with signal-to-noise ratios of SNR = 1 or SNR = 25 demonstrates that the major problem is not the convergence of the fitting routine, but failures of the level detector algorithm which creates the dwell-times distributions from noisy time series.

The macrochannel presentation allows the incorporation of constraints like channel interaction. The evaluation of simulated 4-channel records in which the rate-constant of opening increased by 20% per already open channel could reveal the interaction factor.

Correspondence to: U.-P. Hansen

Abbreviations: p.d.f. = probability density function of the durations of sojourns at the conductance level.

Key words: Channel interaction — Dwell-time histograms — Markov process — Rate constants — Target-fit

Introduction

Channels in biological membranes are mostly described by aggregated Markov processes (Colquhoun & Hawkes, 1977, 1981, 1982, 1987, 1990, 1995; Korn & Horn, 1988; Neher & Stevens, 1977; Yeo et al., 1988; Ball & Rice, 1992). This means that the gating behavior of a channel is described by spontaneous jumps between discrete states, which may differ in their conductance. The aim of a kinetic analysis is to evaluate the arrangement of the states and the transition rates.

A minority of workers make use of the deviations from Gaussian distributions in amplitude distributions by an analysis based on beta distributions (FitzHugh, 1983; Yellen 1984; Klieber & Gradmann, 1993).

The majority prefers the analysis of the measured temporal behavior of the patch clamp current, and a great variety of methods is employed. Some algorithms deal with each data point of the time series, others make use of pre-averaged data that enter the calculations as one- or two-dimensional dwell-time distributions. Dwell-time distributions give the probability that a given duration of a sojourn in a certain state will be observed. If the probability distribution of the length of these sojourns is dependent on the dwell-time in the preceding state(s), higher-dimensional dwell-time distributions are used. Another difference between approaches is in their capability to account for the effects of missed events and noise.

Another feature which renders the evaluation of single-channel rate constants from dwell-times difficult is the fact that channels often occur in clusters. This aggregation is probably brought about by binding to membrane-associated guanylate kinases, as shown by Kim et al. (1995) for Shaker-type K^+ channels. The in-

volvement of the cytoskeleton is also indicated by the observation that single-channel records can be obtained if cytochalasin is given which makes the channels spread (Pongs, *personal communication*). This cluster formation may be the origin of rarely observed channel interaction (Yeramian, Trautman & Claverie, 1986; Manivannan et al., 1992; Draber, Schultze & Hansen, 1993; Liu & Dilger, 1993).

The majority of tools for the evaluation of patch-clamp data is tailored for single-channel dwell-time distributions (Ball & Sansom 1989; McManus and Magleby, 1989; Magleby & Weiss 1990*a*,*b;* Ball, Milne & Yeo, 1993; Colquhoun, Hawkes & Srodzinski, 1996). It is difficult to interpret the data obtained from the fits of multichannel records in terms of single-channel parameters. Thus, the analysis of the kinetics of gating is often restricted to:

– single-channel records or multichannel records with sections of only one active channel;
– fast flickering (Draber et al., 1993);
– evaluation only of the states ''all channels open'' or ''all channels closed'' thus using the dwell-time histograms with the smallest number of events and a low statistical significance.

The restriction to single-channel records leads to the rejection of many experiments. However, there are powerful approaches for multichannel analysis, e.g., the direct fit of the time series. The required computer time could be limited to hours or days by using a one-step prediction algorithm. The approach of Horn and Lange (1983) was already a multichannel analysis, which was based on recursive one-step prediction of the composition of open states. A missed-events correction was introduced later. It was approximate (Sine, Claudio & Sigworth, 1990) or exact (Colquhoun et al., 1996), but in both cases it was restricted to single-channel analysis with a constant dead time which ignores the effects of noise and of the memory of the detector (Magleby & Weiss, 1990*a*).

The potential for implementing all desirable options is provided by the method of Fredkin and Rice (1992) which was extended to multichannel analysis by Albertsen and Hansen (1994) and Klein, Timmer and Honerkamp (1997). Here, also the states of the involved channels are predicted. However, in contrast to the approach of Horn and Lange (1983) the calculation of the likelihood is not based on the probability that the predicted state does occur, but that the measured current can be assigned to the predicted state. This provides two benefits: Firstly, a jump detector is avoided. Level detection is still employed as the overall amplitude histogram has to be split into partial amplitude distributions that provide the probability that a measured current is related to a certain level. Secondly, noise is accounted for because the width of the partial amplitude histograms determines the probability that the measured current is related to the predicted state. Furthermore, filtering can be included by splitting multistate multichannel beta distributions into partial amplitude histograms (FitzHugh, 1983; Yellen, 1984). The algorithms for multistate multichannel histograms have been furnished by Riessner (1994).

However, the prediction of the time series and the simulation of two-dimensional dwell-time distributions require computer time which ranges from several hours to several days (Magleby & Weiss 1990*b*; Albertsen & Hansen 1994) for just one patch-clamp record. The problem of computer time seemed to be overcome by Qin, Aucherbach and Sachs (1996) who used the reconstructed time series for the prediction algorithm. However, here again a jump detector had to be employed, and the missed-events correction was based on a multichannel extension of the approach of Roux and Sauvé (1985) which does not account for the memory of the detector (filtering).

The required computer time may become a problem if great amounts of data have to be analyzed. An example that illustrates the need of a faster approach is the study of the fast-blocking effects of metal ions on the K^+ channel in *Chara* (Draber & Hansen, 1994; Hansen, Keunecke & Blunck, 1997) with a sampling rate of 200 kHz: 2 million data points are stored on disk every 10 sec. Most of the records include more than one channel.

Secondly, besides the extreme computer time required by the direct fit of the original time series, there is another problem that may be considered to be just of psychological origin, but many workers will feel that this is important: the investigator has to rely completely on the computer algorithm because the whole analysis of the direct fit occurs ''in a long dark tunnel.'' The investigator starts the fitting routine and gets just a handful of numbers (4 to 10 rate constants k_{ij}) at the end of the tunnel after 1 to 100 *hr*. There is no visual control of the progress of the fitting process. In the case of dwell-time distributions, there are diagrams with clouds of data points with more or less pronounced curvature, and the computer draws lines through these clouds. Then, the researcher can judge by eye whether this fit is convincing or not, and weighting factors may be employed to improve the fit.

The above reasons, but also the widespread use of dwell-time distributions (Colquhoun & Hawkes, 1995) led to the desire of a multichannel fit of dwell-time distributions. The requirement of computer time can be reduced if a lower degree of sophistication is accepted.

The price that has to be paid for higher speed is as follows: Firstly, the analysis of one-dimensional dwell-time distributions ignores the information comprised

in internal correlation (Fredkin, Montal & Rice, 1985). This can be obtained from joint distributions of apparent open and closed times, which describe the dependence of an observed dwell-time in state B on the preceding time in state A (Colquhoun & Hawkes, 1987; Blatz & Magleby, 1989; Weiss & Magleby, 1989; Magleby & Weiss 1990*a,b;* Colquhoun et al., 1996; Rothberg, Bello & Magleby, 1997). Magleby and Song (1992) have shown that Markov models which led to the same maximum likelihood on the basis of one-dimensional dwell-time distributions could clearly be distinguished by means of two-dimensional dwell-time distributions. This reduces the class of indistinguishable models, even though it has to be kept in mind that already simple models may not be distinguished by means of their kinetics (Kienker, 1989). The two-dimensional presentation is also useful to check the reversibility of the underlying process (Song & Magleby, 1994).

Secondly, more serious is the neglect of the missed-events problem (Roux & Sauvé 1985; Blatz & Magleby, 1986; Yeo et al., 1988; Ball & Sansom, 1989; Hawkes et al., 1990, 1992; Colquhoun et al., 1996). This may be regarded as a major disadvantage because a retrospective correction as provided for single-channel records (Crouzy & Sigworth 1990; Draber & Schultze, 1994) is not available for multichannel multistate records.

The restriction of the fitting routine to one-dimensional dwell-time distributions does not necessarily lead to a loss of information if the experiments have produced some single-channel records. They can be used for the construction of two-dimensional dwell-time distributions (Magleby & Weiss, 1990*a,b;* Magleby & Song, 1992; Colquhoun et al., 1996), from which the model for the subsequent fitting of the multichannel one-dimensional dwell-time distributions can be obtained.

Missed-events corrections could be included by using the survivor function R (Ball & Sansom, 1989; Hawkes et al., 1990, 1992; Colquhoun et al., 1996). However, it is questionable whether the gain of accuracy is worth the considerable loss of speed. Firstly, as stated by Magleby and Weiss (1990*a*) ''the matrix methods disregard the effects of noise and make unrealistic (idealized) assumptions about the effects of filtering.'' Filtering (memory of the detector: Draber & Schultze, 1994) and noise (Magleby & Weiss 1990*a,b*) may have effects that exceed that of a detector with constant dead-time (Colquhoun & Hawkes 1990). Thus, the inclusion of the survivor function does not account for all aspects of the missed-events problem. Secondly, there is the option to investigate selected records with more sophisticated methods after a rough picture has been obtained from fitting all data. Because of the restricted number, the best of all available methods can be used. Thirdly, using simulations, Magleby and Weiss (1990*a*) and Colquhoun et al. (1996) have shown that missed events do not add additional time constants (phantom exponentials: Blatz & Magleby, 1986; Yeo et al. 1988) if that part of the dwell-time histogram with $t < 3$ dead times τ_d is omitted. This is mainly the first (which is increasing because of missed events) part of the dwell-time distributions (McManus & Magleby, 1989; Colquhoun et al., 1996). The effects of missed events can be handled by an asymptotic form of the exact equations including the survivor function in the range of $3\ \tau_d < t < 20\ \tau_d$ (Colquhoun et al., 1996). Fourthly, there is hope (McManus & Magleby, 1989) that the error by ignoring missed events results in a parallel shift by apparent rate constants obtained under the influence of different agents. Thus, the effect of an agent can still be characterized.

Because only an incomplete missed-events correction could be incorporated into the analysis of pre-averaged data (dwell-time distributions), researchers may look for a dual strategy for fitting the data: A fast and simple method for the analysis of all data and a slow and sophisticated analysis (e.g., the direct fit of the time series, Albertsen and Hansen, 1994; Klein et al., 1997) for selected records in order to check and/or supplement the rough data of the first run.

For the first run, a method is suggested here which is a modification of that of Kijima and Kijima (1987*b*), which was based on the assumption of identical channels. The new approach is based on a ''macrochannel'' presentation (Colquhoun & Hawkes 1977, 1990), and it makes use of a target fit. The search routine in a target-fit optimizes those parameters which are the ''target'' of the analysis: here, the rate constants of the transitions in a Markov model. The target fit has several advantages over the widely used fit with time constants (Colquhoun & Sigworth, 1983). At first, the calculation of the rate constants from the set of time constants and amplitude factors is very complicated even though the situation is improved by the algorithms suggested by Jackson (1997). Other benefits of this approach are:

– the application to ensembles with nonidentical channels including sublevels;

– global fitting of the dwell-time distributions for all levels in a multichannel record with the same data set;

– global fitting of different experiments: the investigation of the effects of an agent on a certain rate-constant gets more powerful when all rate-constants besides the influenced ones are kept equal in all data sets;

– the simpler inclusion of constraints, e.g., a certain coupling between rate constants as given in the case of cooperativity (Draber et al., 1993; Kiss & Nagy, 1985; McGeoch & McGeoch, 1994).

Even though it is recommended to check the results of the first run by more sophisticated methods, in many cases the results of the one-dimensional dwell-time analysis can be used directly. Thus, it is investigated by

means of simulations, whether the approach presented here can yield results of sufficient quality.

Presenting an Ensemble of Channels by one Macrochannel

The concept of a macrochannel for multichannel analysis has been used already by Colquhoun and Hawkes (1977, 1990). The way from the single channel to the marco channel is illustrated by means of Fig. 1 for an ensemble of two identical channels with three states each, the open state *O* and two closed states *C* and *G* in the following configuration

$$C \underset{k_{OC}}{\overset{k_{CO}}{\rightleftharpoons}} O \underset{k_{GC}}{\overset{k_{CG}}{\rightleftharpoons}} G \qquad (1)$$

According to Fig. 1, the nomenclature (including additional models below) has to distinguish between four different kinds of models:

O, A, C, G	states of the single channel (O, A are open, C, G are closed)
U_j	original states of the marcochannel as obtained by writing down all possible combinations of N individual single channels
R_r	kinetic states (kinetically different) of the macrochannel as described by the **b**-vector (vector of state occupancies) whose Q components give the numbers of involved single-channel states ($1 \leqslant r \leqslant B$)
R	vector consisting of all states R_r
$R_r^{(m)}$	states R_r belonging to one state Y_m
$R^{(m)}$	vector consisting of the states $R_r^{(m)}$
	The above symbols R are also used for the probability of being in state R_r
Y_m	conductance states (aggregated states), which can be distinguished by the measured macrochannel currents ($1 \leqslant m \leqslant M$). All states R_r which lead to the same conductance (same number of open channels) form one state Y_m.

with

Q	number of states in the single channel model(s) if identical channels are considered, otherwise Q_i has to be used in order to account for different channel types i
N	number of single channels
Q_M	number of states in the Markov-model at the left-hand side of Fig. 1
B	number of **b**-vectors (vectors of state occupancies)

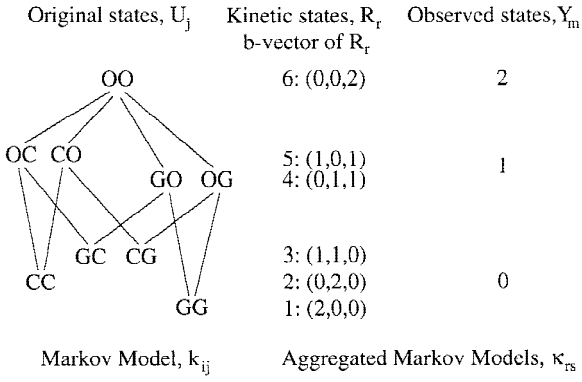

Fig. 1. Different presentations of the marcochannel. On the left-hand side are the states of the original model (2 channels of the *C-O-G* type of Eq. 1). The models in the middle and on the right-hand side are aggregated models. In the middle, the states R_r are represented by the related **b**-vectors (vector of state occupancies). In the case of only one open state, the number m of Y_m is equal to the last element in the **b**-vector.

B_m	number of **b**-vectors related to the macro (conductance) state Y_m
M	number of macro (conductance) states Y_m
$b_i^{(r)}$	ith component of the **b**-vector of state R_r (Eqs. 3,4)

The rate constants are

k_{ij}	for the single channel ($1 \leqslant$ i,j $\leqslant$ Q)
κ_{rs}	for the macrochannel ($1 \leqslant$ r,s $\leqslant$ B).

The Rate Equations

For the change of the probability of being in a kinetic state R_r (which is also called R_r), the following rate equation holds

$$\frac{d}{dt}R_r = -\sum_{\substack{s=1\\ s\neq r}}^{B} \kappa_{rs}R_r + \sum_{\substack{s=1\\ s\neq r}}^{B} \kappa_{sr}R_s = \kappa_{rr}R_r + \sum_{\substack{s=1\\ s\neq r}}^{B} \kappa_{sr}R_s \qquad (2)$$

The form of the rate Eq. 2 is obvious, because the concept of single-channel analysis can be applied to the states R_r of the macrochannel (Fig. 1, middle).

The relationship between the marcochannel rate constants κ_{rs} and the single-channel rate-constants k_{ij} can be obtained from a comparison of the original model on the left-hand side of Fig. 1 and the kinetic model in the middle. If there is a jump from state R_r to state R_s, we call R_r a source state and R_s a sink state. Those states R_s which are eligible as sink states for R_r can be found by considering the related **b**-vectors (vectors of state occupancies). The constraint that the number of channels has to be constant leads to the demand that the vector $\mathbf{b}^{(r)}$ of R_r has to have one channel more in state i ($\mathbf{b}_i^{(r)} = \mathbf{b}_i^{(s)} +$

1) and one less in state j than the vector $b^{(r)}$ of R_r has. Thus,

$$b^{(r)} = b^{(s)} + e_i - e_j \tag{3}$$

with e_i and e_j having a ''1'' at position i or j, respectively, and zeros otherwise. The term $b + e_i - e_j$ is explained by the following example

$$b^{(r)} = \begin{bmatrix} b_1 \\ b_2 + 1 \\ b_3 - 1 \end{bmatrix}^{(r)} = \begin{bmatrix} b_1 \\ b_2 \\ b_3 \end{bmatrix}^{(s)} + \begin{bmatrix} 0 \\ 1 \\ 0 \end{bmatrix} - \begin{bmatrix} 0 \\ 0 \\ 1 \end{bmatrix} \tag{4}$$

In the above jump from R_r to R_s, the second element in the **b**-vector, b_2, is decreased by 1, and the third element b_3 is increased by 1. That means that one channel that has been in the single-channel state 2 jumps into the single-channel state 3.

The states R_r are aggregated Markov states. If $b_i^{(r)}$ is greater than 1, each one of the channels in state i may jump. Thus, the rate constant of the transition from state R_r to R_s has to be multiplied by $b_i^{(r)}$

$$\kappa_{rs} = b_i^{(r)} \cdot k_{ij} \tag{5}$$

i and j have to be obtained from an inspection of the original states as shown in Fig. 1 at the left-hand side.

A jump out of R_r into any state R_s occurs when one of the single states i included in $\mathbf{b}^{(r)}$ changes to a state $j \neq i$. In order to include all possible jumps, a double sum is obtained for the probability $-\kappa_{rr}$ of leaving state R_r

$$-\kappa_{rr} = \sum_{\substack{s=1 \\ s\neq r}}^{B} \kappa_{rs} = \sum_{i=1}^{Q} \sum_{\substack{j=1 \\ j\neq i}}^{Q} b_i^{(r)} k_{ij} \tag{6}$$

The elements in the main diagonal are the negative sum of all other elements in the same row (Colquhoun & Hawkes, 1977, 1987, 1995).

For the jumps into R_r it has to be considered that **b**-vector of the source state R_s has to have one channel more in state j and one less in state i, because a jump from single-channel state j to single-channel state i has to result in the configuration of the vector of state occupancies $\mathbf{b}^{(r)}$ (similar to Eq. 4).

This leads to the necessity of extending the indices of states R_r and R_s (which now are the sink and source states, respectively) by the related **b**-vectors $\mathbf{b}^{(r)}$ and $\mathbf{b}^{(s)}$ of Eq. 3. Using Eqs. 5 and 6 the single-channel rate constants are introduced into Eq. 2.

$$\frac{d}{dt} R_{r,b^{(r)}} = -R_{r,b^{(r)}} \left[\sum_{i=1}^{Q} b_i^{(r)} \sum_{\substack{j=1 \\ j\neq i}}^{Q} k_{ij} \right]$$

$$+ \sum_{i=1}^{Q} \sum_{\substack{j=1 \\ j\neq i}}^{Q} (b_j^{(r)} + 1)\, k_{ji} R_{s,[b_j^{(r)} + e_j - e_i]} \tag{7}$$

In the last sum of Eq. 7, $b_j^{(s)}$ is replaced by $b_j^{(r)} + 1$, according to Eq. 3.

The Steady-state Probabilities of the Macrochannel

$R_r(\infty)$, the steady-state probability of being in state $R(r,b^{(r)})$ is obtained for $dR/dt = 0$ in Eq. 7. A solution of this equation for N identical channels is

$$R_{r,\infty} = \frac{N!}{\prod_{i=1}^{Q} b_i^{(r)}!} \cdot \prod_{i=1}^{Q} p_i^{(\infty) b_i^{(r)}} \tag{8}$$

For the derivation of this equation we have to consider the probability of being in state R_r which is described by the vector $\mathbf{b}^{(r)}$. The probability of a single channel to be in state i is $p_i(\infty)$. As this state has to occur $\mathbf{b}_\mathbf{i}^{(r)}$ times, the exponent $\mathbf{b}_\mathbf{i}^{(r)}$ is introduced. Now it has to be considered how many combinations of the N channels would result in $b_i^{(r)}$ channels in state i. The derivation is simple if we start with an ensemble of N channels which have $Q = N$ states. Then, we consider the special state R_a which is described by the **b**-vector $\mathbf{b}^{(a)} = (1,1,1.\,.1)$, i.e. all $b_i^{(a)} = 1$. There are $N!$ permutations of the $Q = N$ states to fill the $Q = N$ components of that vector.

In all other **b**-vectors (vectors of state occupancies) of this ensemble, the occupancies of the bins are not so evenly distributed. Some of the ''1''s are taken out of some bins (components) and collected in other bins. In these bins with multiple occupancy, the $b_j^{(r)}$ channels of equal state j can no longer be distinguished. Thus, the number of permutations, which is $N!$ in $b^{(a)}$, is decreased by a factor of $b_j^{(r)}$!, and Eq. 8 is obtained. With other words, the first factor in Eq. 8 gives the number of kinetically equivalent arrangements of the N channels leading to the same vector $\mathbf{b}^{(r)}$.

This consideration applies also to ensembles with the number of states Q that is smaller than the number of states N. In that case, N-Q components of an extended **b**-vector are set to zero. As a consequence of the reduced number of occupied places in the **b**-vector, the available places have to have multiple occupancies. This leads to $b_i^{(r)} > 1$, and the scenario is equal to that described above.

In addition to the above considerations, the correctness of Eq. 8 is tested in Appendix I by showing that it is a solution of Eq. 7 for $dR/dt = 0$.

The Probability Density Functions (p.d.f.) of Sojourns in the States of the Macrochannel

The matrix form of the rate equations of the example in Fig. 1 is as follows

$$\frac{d}{dt}\left[\begin{bmatrix}R_1\\R_2\\R_3\end{bmatrix}\begin{bmatrix}R_4\\R_5\end{bmatrix}[R_6]\right]^T$$

$$= [\overline{\underline{R_1R_2R_3}}\ \overline{\underline{R_4R_5R_6}}] \cdot \begin{bmatrix} \overline{|\kappa_{11}\kappa_{12}\kappa_{13}|}\ \kappa_{14}\kappa_{15}\kappa_{16} \\ |\kappa_{21}\kappa_{22}\kappa_{23}|\ \kappa_{24}\kappa_{25}\kappa_{26} \\ |\kappa_{31}\kappa_{32}\kappa_{33}|\ \kappa_{34}\kappa_{35}\kappa_{36} \\ \kappa_{41}\kappa_{42}\kappa_{43}\ \overline{|\kappa_{44}\kappa_{45}|}\ \kappa_{46} \\ \kappa_{51}\kappa_{52}\kappa_{53}\ |\kappa_{54}\kappa_{55}|\ \kappa_{56} \\ \kappa_{61}\kappa_{62}\kappa_{63}\ \kappa_{64}\kappa_{65}\ \underline{|\kappa_{66}|} \end{bmatrix} \quad (9)$$

with κ_{rs} obtained by Eq. 5.

The full equation is required for the determination of steady-state concentrations R_r. In the case of identical channels, the solution is given by Eq. 8.

For the p.d.f. $y_m(t)$ of the duration of sojourns in the state Y_m, the reduced equation of the absorbing system (Kijima & Kijima, 1987*a*) is required. Jumps into the state R_r must occur only from substrates R_s if the jumps do not change the conductance. Thus, these source states have to belong to the same index m of the current state Y_m (right-hand side of Fig. 1). In Eq. 9, the aggregation of the substrates R_r belonging to one phenomenological macrostate Y_m are indicated by the brackets on the left-hand side or by overlining and underlining in the middle.

An inspection of the matrix multiplication shows that in the reduced rate equations only those κ_{rs} are involved which are surrounded by boxes. Even though jumps out of Y_m may go to all sink states, they are also included in the boxes. This is a consequence of the fact that the number of jumps out of the level has to be equal to the number of jumps into the level (Colquhoun & Hawkes, 1995). Thus, the elements in the main diagonal are the negative sum of all other elements in the same row (Eq. 6).

$$\kappa_{rr} = -\sum_{\substack{s=0\\ s\neq r}}^{B} \kappa_{ij} \quad (10)$$

κ_{rr} on the diagonal includes all these transitions out of R_r. Thus, the whole behavior of the reduced rate equations can be described by the submatrices ($B_m \times B_m$) surrounded by boxes.

The eigenvalues $\lambda_i^{(m)}$ of the submatrices K_m related to one state Y_m (with the states $R_r^{(m)}$) are obtained from the solutions of the reduced equation (boxes in Eq. 9) of the absorbing system

$$\lambda_i^{(m)} (v^{(m,i)})^T = (v^{(m,i)})^T \cdot K^{(m)} \quad (11)$$

The eigenvector $v^{(m,i)}$ ($1 \leqslant i \leqslant B_m$, and the additional first index m indicates the assignment of the B_m eigenvectors $v^{(m,i)}$ to the macrostate Y_m) consists of the components

$$(v^{(m,i)})^T = [v_1^{(m,i)}, v_2^{(m,i)}, v_3^{(m,i)}, \ldots\ldots\ldots v_{B_m}^{(m,i)}] \quad (12)$$

Because of the segmentation of the full K-matrix into submatrices (Eq. 9), the B_m eigenvectors $v^{(m,i)}$ are determined only by the ($B_m \times B_m$) submatrices. The determination of the eigenvectors $v^{(m,i)}$ only by the rate constants κ_{rs} belonging to this state Y_m avoids interference with eigenvectors of other macro-states $Y_{m'}$.

The macrochannel consisting of the kinetic R-states is an aggregated Markov model. Because of this, the solution for single-channel p.d.f.s can be used (Kijima & Kijima, 1987*a*). For this single-channel, the p.d.f. of the closed state (superscript c) y_{JSh} is

$$y_{JSh}(t) = \sum_{i\epsilon closed} d_i^{(c)}\, e^{-\lambda_i^{(c)} t} \quad (13)$$

$$d_i^{(c)} = 2S^{(c)} \left(\sum_{I\epsilon closed} p_I(\infty)\, v_I^{(c,i)} \left(\sum_{J\epsilon open} k_{I,J} \right) \right)^2 / \overline{f_{tr}} \quad (14)$$

with *JSh* (just shut) indicating that the channel that has closed at time zero and opens at time t. $\lambda_i = 1/\tau_i$ are the eigenvalues of the reduced matrix K′related to the ensemble of closed states as shown by the boxes in Eq. 9. $v_i^{(c,i)}$ is the I-th component of the eigenvector of the reduced matrix K' of the closed state. $S^{(c)}$ is the scaling factor. The probabilities are normalized by dividing by $\overline{f_{tr}}$, the number of all transitions in the record divided by the sampling time.

In contrast to the single-channel analysis, there is no longer a distinction between open and closed states in the analysis of the macrochannel. It is replaced by a distinction of the current states Y_m (Fig. 1).

The channel jumps into the level Y_m at $t' = 0$ and stays there until time $t' = t$. At $t' = t$ it jumps out of the level m. The p.d.f. $y_m(t)$ for the dwell-times in Y_m is:

$$y_m(t)\, dt = \sum_{i=1}^{B_m} d_i^{(m)}\, e^{-\lambda_i^{(m)} t}\, dt \quad (15)$$

$$d_i^{(m)} = 2S_m \sum_{r\epsilon Y_m} R_r^{(m)}(\infty)\, v_r^{(m,i)} \cdot \left(\sum_{r\epsilon Y_m} \sum_{s\notin Y_m} \kappa_{rs} \right)^2 / \overline{f_{tr}^{(m)}} \quad (16)$$

Y_m comprises all states R_r belonging to one m-state (submatrices in Eq. 9). B_m gives the number of the different kinetic states comprised in the aggregated state Y_m · $R_r(\infty)$ is the steady-state probability of R_r · $\overline{f_{tr}^{(m)}}$ is the average transition frequency for the macrochannel. Because of the macrochannel approach of Fig. 1, it can be derived similar to that of the single-channel model (Kijima & Kijima, 1987*a*)

$$\overline{f_{tr}^{(m)}} = 2 \sum_{r \in Y_m} R_r^{(m)}(\infty) \cdot \sum_{s \notin Y_m} \kappa_{r,s}\, \kappa_{s,r} \tag{17}$$

The Scaling of the p.d.f.

The scaling factor of the p.d.f.s, S_m, is obtained from the conditions of normalizing the eigenvectors of the reduced matrix. The probability of being in the macrochannel level Y_m is

$$p_m = \frac{T_m}{T} \tag{18}$$

with T_m being the overall dwell-time in level Y_m and T the overall duration of the experiment. T_m is obtained from the m-th p.d.f.

$$T_m = S_m \int_0^\infty \sum_{r=1}^{B_m} t\, d_i^{(m)} \cdot e^{-\lambda_i^{(m)} t}\, dt = S_m \sum_{i=0}^{B_m} \frac{d_i^{(m)}}{\lambda_i^{(m)2}} \tag{19}$$

with S_m being the scaling factor.

Replacing T_m in Eq. 19 by Eq. 18 leads to

$$S_m = \frac{p_m \cdot T}{\sum_{i=1}^{B_m} \frac{d_i^{(m)}}{\lambda_i^{(m)2}}} \tag{20}$$

Since the temporal resolution of the measured dwell-time histograms is given by the sampling period T_s, Eq. 15 has to be integrated over the range of one bin. Assuming that d_m is constant within one bin, the integration can be replaced by multiplying d_m with T_s.

$$S_m = \frac{p_m \cdot T \cdot T_s}{\sum_{i=1}^{B_m} \frac{d_i^{(m)}}{\lambda_i^{(m)2}}} \tag{21}$$

The probability p_m of being in state Y_m is the sum of the probabilities $R_r(\infty)$ of being in one of the substates R_r belonging to Y_m

$$S_m = T_s \cdot T \cdot \frac{\sum_{r=1}^{B_m} R_r^{(m)}(\infty)}{\sum_{i=1}^{B_m} \frac{d_i^{(m)}}{\lambda_i^{(m)2}}} \tag{22}$$

A Computer Program for a Target Fit of the Multichannel p.d.f.s.

Because of the linearity of Markov processes, dwell-time histograms obtained from an ideal detector (without limited resolution) have always to be fitted by a sum of exponentials (Eq. 15). In the case of filtering, terms of the form $t^n \exp(t/\tau)$ are obtained. However, the exponential terms are a good approximation if the p.d.f. starts at $t >$ three dead times τ_d (Colquhoun et al. 1996; Magleby & Weiss, 1990*a*), but the evaluated time constants may be biased. By means of the following simulations it is investigated how serious this bias is.

An important difference between fitting strategies lies in the parameters which are delivered. Usually, the amplitude factors d_i and time constants $\tau_i = 1/\lambda_i$ are obtained. However, the optimum ''target'' of the analysis should be the set of rate constants k_{ij}. In simple cases, some of them can be obtained from the inverse time constants of the closed states ($\tau_i = 1/\Sigma k_{ij}$, Colquhoun & Hawkes, 1995), but the relationships are highly complicated in most cases (Jackson, 1997). In a target-fit, the rate-constants are determined directly.

The program developed for the target fit of the p.d.f.s of the macrochannel enables the fit of ensembles of up to 11 to 3 identical single-channels with up to 2 to 5 states, respectively. These states may be ''open'', ''sublevel'' or ''closed''. So far, the program is restricted to two classes of open states which are related to two different conductances.

The program (flow diagram is shown in Fig. *A*1 in Appendix II) starts with the specification of the single-channel model. The user enters the number of all states Q, the number of open states (Q_{op}) and of sublevel states (Q_{sub}). There is the convention, that the first states are open ones. In the middle are the sublevel states, and the closed ones are the last ones.

After assigning the states, the computer has to know from which single-channel state to which single-channel state transitions may occur. For this purpose, the program prepares a $Q \times Q$ matrix. The model is selected by specifying the transitions k_{ij} in this matrix. This is done by assigning nonzero numbers to the selected transitions. Normally, the values of these numbers are less important. However, since these numbers are used as starting values of the k_{ij} in a subsequent fitting routine, the fitting procedure runs better if these values are similar to those known from other experiments or from a reasonable guess.

For the creation of the B × B K-matrix of the macrochannel, a two-dimensional array of states of the size $(Q + 1 + Q_o) \times B$ comprising all $b^{(r)}$-vectors of the states R_r has to be generated. An example of the array is given in Table 1 for an ensemble of three 3 *O S C G F* — channels with the last three states being nonconducting. Q_o is the number of different single-channel conductance levels. The first Q_o components in the rows give the numbers of channels in the different conductances states (full conductance and subconductance in the example of Table 1). Blocks of rows with equal (m_{op}, m_{sub})-entries

Table 1. An example of the array of states for an ensemble of three *O-S-C-G-F* channel with O = full conductance and S = subconductance

m_{op}	m_{sub}		bm	$b_1^{(r)}$	$b_2^{(r)}$	$b_3^{(r)}$	$b_4^{(r)}$	$b_5^{(r)}$	r	dec
	0	0	1	0	0	0	0	3	1	3
			2	0	0	0	1	2	2	6
			3	0	0	0	2	1	3	9
			4	0	0	0	3	0	4	12
			5	0	0	1	0	2	5	18
			6	0	0	1	1	1	6	21
			7	0	0	1	2	0	7	24
			8	0	0	3	0	0	8	48
	0	1	1	0	1	0	0	2	9	66
			2	0	1	0	1	1	10	69
			3	0	1	0	2	0	11	72
			4	0	1	1	0	1	12	81
			5	0	1	1	1	0	13	84
			6	0	1	2	0	0	14	96
	0	2	1	0	2	0	0	1	15	129

etc.

The column r is the address of the row in the matrix K of Eq. 9. dec ist the decimal value of the counter.

are combined to give one Y_m state. bm counts the individual **b**-vectors (vectors of state occupancies) belonging to one Y_m. The last number bm in such a block is B_m. The other elements of the row are the components of the related **b**-vector. r is the address of this row of the array. It is also the index of the related state R_r.

For the generation of the array of Table 1, a counter is employed. This counter does not use the decimal system, but a system with the basis $(N + 1)$. A **b**-vector is a number ${}_{(\mathbf{N}+1)}n$ in this $(N + 1)$ system (the occupancies of $b_i^{(r)}$ can be 0 to N) with Q digits. However, not all numbers ${}_{(N+1)}n$ are valid **b**-vectors.

The selection of **b**-vectors and their assignment is done as follows: *bm* is set to zero, and the counter starts with ${}_{(N+1)}n = 1$ and continues to ${}_{(N+1)}n = (N + 1)^Q$ (actually it is stopped as soon as the last digit has reached $N + 1$ ($b_Q^{(\mathrm{rmax})} = N + 1$), because the subsequent numbers cannot be valid **b**-vectors as the number of channels would be greater than N).

At each counting step, an if-statement asks whether the sum of all digits is N

$$\sum_{i=1}^{Q} b_i^{(r)} = N? \tag{23}$$

because the sum of the digits is the number of channels in the ensemble, and this always has to be N.

If the answer is yes, the indices m_{op} and m_{sub} are determined by adding the digits belonging to the open states and to the substates, respectively. The element bm in the third component of Table 1 is increased by one. It is set back to one when m_{sub} or m_{op} change. $b_1^{(\mathrm{r})}$, . . $b_Q^{(\mathrm{r})}$ are filled with $b_i^{(r)}$ taken from the actual ${}_{(N+1)}n$ number (which has fulfilled the condition of Eq. 23). At the end of the counting procedure, the array is filled.

The construction of the $B \times B$ macrochannel **K**-matrix (Eq. 9) starts with the empty matrix (B = number of all R_r states). To find the entries of the s-th column (elements κ_{rs} with $r = 1$ to B and $s \neq r$), $\mathbf{b}^{(s)}$ is compared with all vectors $b^{(r,mop,msub)}$ of possible source states R_r in the array of states. Those vectors $\mathbf{b}^{(r)}$, which fulfill the relationship of Eq. 3 lead to nonzero entries as given by Eq. 5 and 6. Having finished the creation of the macrochannel K-matrix, the steady-state concentrations $R_r(\infty)$ can be calculated by means of Eq. 8.

For the solution of the rate-equations of the reduced system (Eqs. 7 and 11), the bookkeeping indices m_{op} and m_{sub} are used to find the submatrices belonging to the state Y_m. The eigenvalues are calculated by a routine in the package ''Eispack'' obtained from the internet.

The procedure described above is embedded in a fitting routine which changes the k_{ij} until the difference between the theoretical and the measured p.d.f.s reaches a minimum. According to our experience with fitting data of biological systems, the most successful nonlinear fitting routine is the Simplex algorithm (Caceci & Cacheris, 1984; Press et al., 1987). The fitting routine is part of our patch analysis program day.pas which is available on request.

Test by Application to Simulated Data

To study the strength of the multichannel analysis, tests with simulated data were performed. A time series of simulated patch current (as described below) was generated from an ensemble of channels with known states and known rate constants and superimposed by red noise with SNR (signal-to-noise ratio) = 1 or SNR = 25. From these noisy records, the noise-free time series was reconstructed by means of a 4th order Hinkley detector (Schultze & Draber, 1993; Hansen et al., 1995). The software of the Hinkley detector also provided bookkeeping of the transitions in order to create the ''experimental'' dwell-time histograms $y_m(t)$ for each level Y_m of current.

In the case of multichannel simulations, the kinetic states of a macrochannel (Fig. 1, middle) were used. The rate constants were entered as rate constants of this macrochannel according to Eqs. 5 and 6. The benefit of this approach is the simple introduction of special effects like channel interaction as illustrated below.

Simulations were done as follows. The program started in level zero (all channels closed). Then, a random generator delivered two numbers. The first one was used to calculate the time of the next jump from the source state to the sink state (continuous time). The dwell-time distribution of the source state R_r is

$$y_r(t) = 1 \cdot \exp(-\lambda_r\, t) \text{ with } -\kappa_{rr} = \lambda_r = \sum_{s \neq r} \kappa_{rs} \tag{24}$$

s labels all possible sink states for a jump out of the present state R_r. The amplitude factor ''1'' is used because the random numbers are equally distributed between 0 and 1. The first random number n_1 was used as an entry of the ordinate of Eq. 24, and the related value t_j at the abscissa is taken as the time of the jump (Press et al., 1987).

$$t_j = -\frac{1}{\sum_{r \neq s} \kappa_{rs}}\, ln(n_1) \tag{25}$$

Now, the second random number n_2 (equally distributed, $0 \leqslant n_2 \leqslant 1$) was used to give the aim (sink state s) of the jump. The interval between 0 and 1 was divided into sections κ_{rs}/λ_r (Eq. 24). That state R_s was selected in whose section n_2 happened to fall. After this jump, the algorithm started again from this new state by generating two new random numbers.

The effect of the anti-aliasing filter was introduced as follows: The jump caused a response of the 4-pole Bessel anti-aliasing filter which was taken out of a memory where jump responses of the anti-aliasing filters were stored. Thus, the series of jumps created by the random generators resulted in a sum of delayed filter responses

$$I(t) = \sum_{j=1}^{W} I_{rs,j} - I_{rs,j}\,(1 - h(t - t_j)) \tag{26}$$

with $I_{rs,j}$ being the step in current related to the jump from state R_r before the jump to the state R_s after the jump at time t_j; t_j is given in continuous time (Eq. 25), and mostly does not coincide with the sampling points. Then, $h(t - t_j)$ is obtained from interpolation of the stored values of $h(t)$. The upper limit of the sum in Eq. 26 is determined by the time t_b that is required by $(1 - h(t))$ to decrease below one bit of the DA converter. Responses of jumps which had occurred before $t - t_b$ were ignored.

This procedure resulted in a much shorter computing time for the calculation of a time series of 2,000,000 samples than a decision at every sampling point if and where to jump. In addition, this program generated a continuous Markov process, as natural channels do. This automatically includes multiple jumps in a sampling period T_s.

The generated time series was superimposed by noise. White Gaussian noise was generated by a Box-Muller algorithm (Press et al., 1987). Filtering in order to obtain white, red or blue noise could be done by digital filtering. In the simultaneous red noise (prefiltered by the same filter $h(t)$ as used in Eq. 26) was used. As always the same time course of the noise was used in the simulations, (variations occurred only in the time series of the ''channel''), the whole time-series of noise was stored in the computer. For composing a noisy patch-clamp record, the freshly prepared channel time series was added to the stored noise series with the same anti-aliasing filter. The signal-to-noise ratio was defined by

$$SNR = \left(\frac{I_o}{\sigma}\right)^2 \tag{27}$$

The assumed sampling rate was 200 kHz, and the anti-aliasing filter was a 4-pole Bessel filter with a corner frequency of 50 kHz.

The first set of simulations was done with 1 to 8 identical channels with the following configuration (rate constants in sec^{-1})

$$\begin{array}{ccccc} & k_{OC} = 100 & & k_{GO} = 1000 & \\ C & \leftrightarrows & O & \leftrightarrows & G \\ & k_{CO} = 50 & & k_{OG} = 500 & \end{array} \tag{28}$$

Fig. 2*A* shows a section from the time series of a 4-channel simulation run with a signal-to-noise ratio (SNR) of 1.

The time series were fed into the program which is presented in the flow diagram of Fig. A1. Firstly, the current levels of the Y_m were determined by positioning horizontal lines in the original time series (fit by eye). Then, these levels were used as starting values for a fit of the amplitude histograms by a sum of Gaussian distributions. The variances σ and the levels were used for the settings of the jump detector. For the reconstruction of the noise-free time series (smooth line Fig. 2*A*), a 4th-order Hinkley detector (Hansen et al., 1995; Schultze & Draber, 1993) was employed. The Hinkley detector program also did bookkeeping of the recorded jumps and created the histograms as shown in Fig. 2 *B–F* for the 5 levels with none to four channels open.

Fitting of these dwell-time histograms with Eqs. 15 and 16 resulted in the smooth lines in Fig. 2 *B–F*. The fit seems to be quite good for level 0 to level 3. In the case of level 4 (Fig. 2*F*) it has to be taken into account that the numbers of events are quite low. Noninteger numbers below 1 event result from presenting average numbers per dwell-time unit. Numbers below one imply that many bins were empty.

The crucial question is whether the fitting routine can reveal the original rate constants which were used to generate the simulated data. In order not to depend on the statistical uncertainty of a single experiment, the simulations were done 100 to 200 times. Even though the same program was used for their generation, time courses were different because of the involvement of the two random generators. Histograms of the distributions of the evaluated rate constants were obtained by plotting

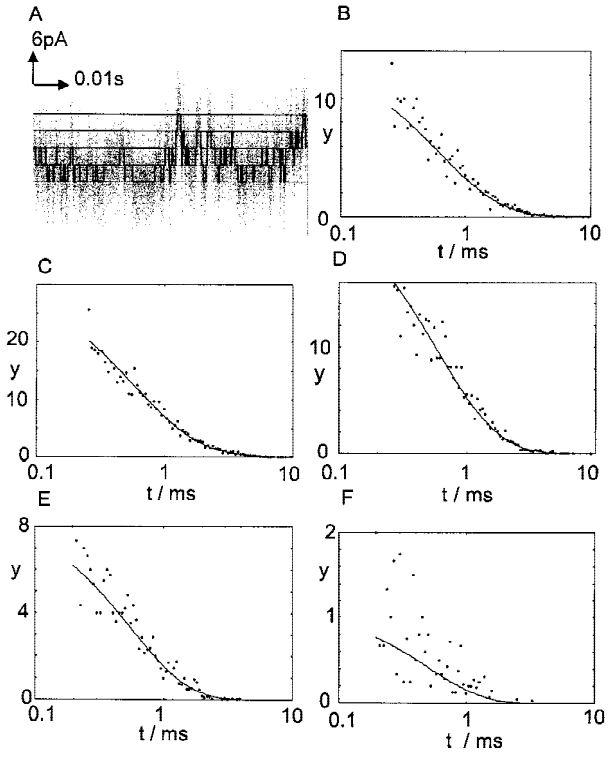

Fig. 2. Section of the time series of a *C-O-G* model with four channels. (Fig. 1*A*) and fits of the dwell-time histograms of current level 0 (*B*) to level 4 (*F*) with 4 channels by means of Eq. 15. The histograms are represented on a logrithmic scale, but the ordinate gives the number of events in a bin divided by the width of that bin. The length of the bins increased exponentially with *t* in order to give an adequate scaling of fast and slow components and in order to give nearly equal statistical weight to fast and slow components in the error sum of the fitting routine. For the simulations, the rate constants given in Eq. 28 were used. Sampling rate was 200 kHz. $2 \cdot 10^6$ data points in a time series with *ca.* 14,000 transitions. Anti-aliasing filter: 50 kHz. A sojourn in a level is ended by a jump upwards or by a jump downwards. The smooth lines present the fits on the basis of Eqs. 15 and 16.

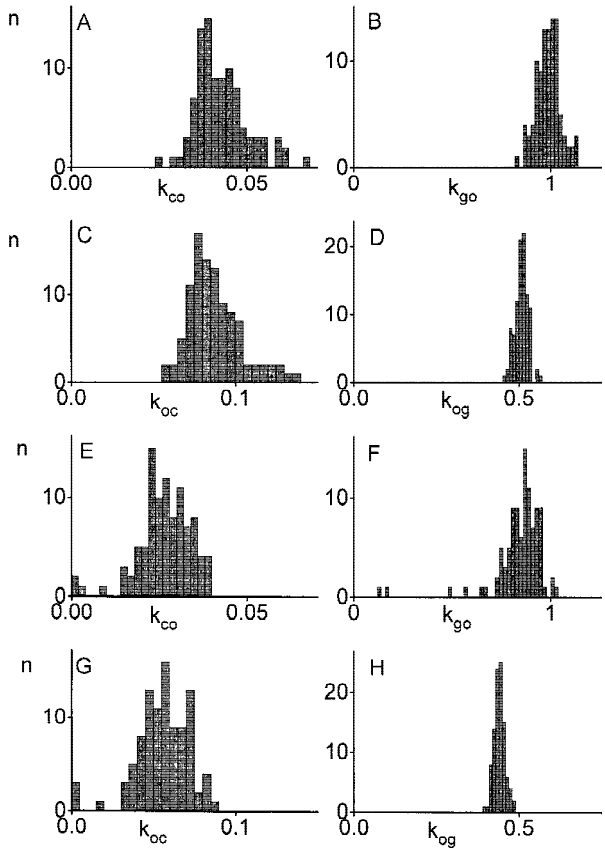

Fig. 3. Histograms of the single-channel rate constants of a *C-O-G* model (Eq. 28) resulting from fitting dwell-time distributions like those in Fig. 2. The data were obtained from 100 simulations of a 4-channel model with the rate-constants given in Eq. 28. (*A*) to (*D*): SNR = 25, (*E*) to (*G*): SNR = 1 (noise filtered by $h(t)$ of Eq. 26). The mean values (in 1/msec) are the numbers at the abscissa in (*A*) to (*D*). The mean values and the standard deviations σ are also given in Table 2.

the number of simulations which led to a rate constant in the bin from k_{ij} to $k_{ij} + \Delta k_{ij}$ (Δk_{ij} is indicated by the width of the columns) *vs.* k_{ij}.

The results obtained from a model with 4 channels of the configuration as given by Eq. 28 are shown in Fig. 3. The upper four histograms of the single-channel rate constants (k_{ij}) were obtained with a SNR of 25, the lower four with SNR = 1. SNR = 1 is a worst-case consideration, as in our lab data sampled with 200 kHz and filtered by a 50-kHz filter reached a SNR of 2 to 3 (Hansen et al., 1997).

In the case of SNR = 25 (nearly noise-free), the multichannel analysis with 4 channels (Fig. 3 *A–D*) gave results which were of equal quality as those obtained for one channel with SNR = 1 and SNR = 25 (histograms not shown, because they were not different from those in Fig. 3 *A–D*, but averaged values are given in Table 2).

However, the results get worse in the presence of strong noise (Fig. 3 *E–H*). Most of the ''experiments'' gave satisfactory results, but there were some failures as indicated by the isolated ''off peak'' events in Fig. 3 *E,F,G*.

The increase of the channel number from 4 to 8 causes problems in the case of noisy data (Fig. 4). Figure 4 *A–D* (SNR = 25) shows good results besides some off-peak values with easily could be eliminated by a visual inspection of the fitted p.d.f.s. However, in the case of SNR = 1 the scatter is tremendous (Fig. 4 *E* to *H*).

This high scatter does not seem to be a failure of the multichannel analysis of Eq. 15, but of the jump detection algorithms. This is illustrated in Fig. 5. Here the rate constants were decreased by a factor of 5 (rate constants in $\sec^{-1}$).

$$C \underset{k_{CO}=10}{\overset{k_{OC}=20}{\leftrightarrows}} O \underset{k_{OG}=100}{\overset{k_{GO}=200}{\leftrightarrows}} G \tag{29}$$

Table 2. Comparison of the mean values (in sec^{-1}) obtained from fitting the 3-state models of Figs. 3 to 5

Rate constants/sec^{-1}			k_{CO}	σ	k_{GO}	σ	k_{OC}	σ	k_{OG}	σ
Nominal			50		1,000		100		500	
ch	SNR	MS								
1	25	2	40	5	992	51	88	13	507	26
1	1	2	36	5	930	53	79	12	446	26
4	25	2	43	7	990	60	88	2	501	20
4	1	2	28	12	841	130	55	16	441	17
8	25	2	40	24	972	157	83	52	508	53
8	1	2	61	87	815	1521	159	665	380	255
Nominal			10		200		20		100	
8	1	10	8	5	187	38	15	11	96	10

ch = numbers of channels, SNR = signal-to-noise ratio (Eq. 27), MS = 10^6 samples.

To compensate for the reduction of the number of events, the number of samples was increased to 10^7. In Fig. 5, the results are much better than in the lower part of Fig. 4.

The reason for the difference in fit quality of Fig. 4 and 5 gets obvious in Fig. 6. Here, the measured p.d.f.s. are compared with those calculated on the basis of Eq. 15 from the original rate constants for the fits in Fig. 4 and in Fig. 5. Since the smooth lines in Fig. 6 are not fits, but the ''true'' curves, the difference between the smooth lines and the data points is an indication of the failure of the jump detection algorithm in the case of noisy data.

The temporal resolution of the Hinkley detector is automatically adjusted to the SNR to keep the number of false alarms below a level of 1 per 10^4 samples (Schultze & Draber, 1993). Thus, the number of missed events increases dramatically in the case of high noise. Figure 6 shows that the ''slow'' channel of Fig. 5 (Eq. 29) can be detected with small errors, but that in the case of the ''fast'' system of Fig. 4 (Eq. 28), the dwell-time distributions delivered by the detector are wrong. The number of detected fast events is too low. In the case of the nearly noise-free data of the upper half of Fig. 4, the dwell-time distributions were okay (*not shown*) because the noise-dependent temporal resolution was much better. These data show again that it is noise which determines the temporal resolution of patch clamp recordings.

To compare the results of Figs. 3–5, the mean values and the standard deviations of the histograms in Figs. 3 to 5 are displayed in Table 2. The upper line gives the ''true'' values as used for the simulation program.

Table 2 shows that the mean values of the histograms are not so far away from the ''true'' values, even in the case of the noisy 8-channel data of Fig. 4 *E–H*. Mostly the difference is 10 to 20%. However, even an error of 50% may be accepted. This is still a ''good'' result according to our experience obtained from fitting of biological systems.

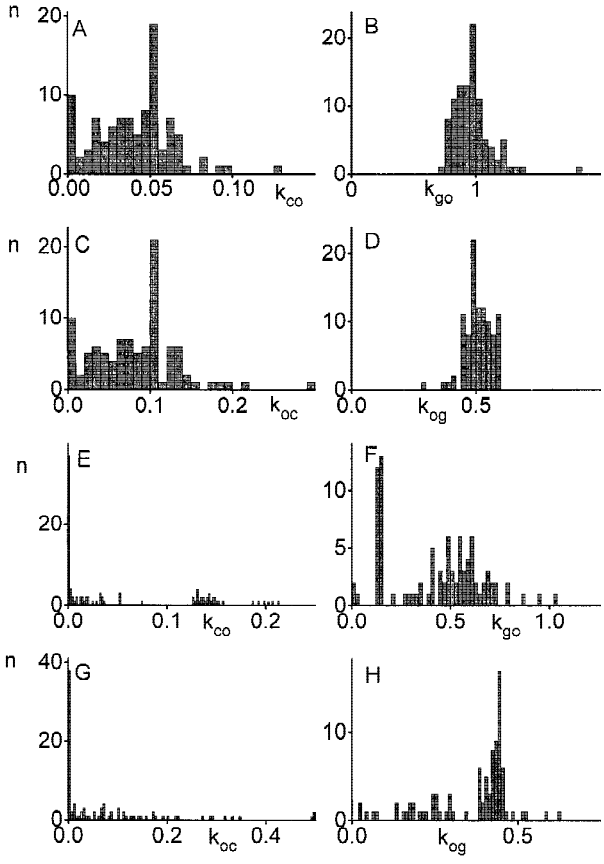

Fig. 4. Histograms of the single-channel rate constants of a *C-O-G* model obtained from 145 simulations of model with 8 identical channels as specified in Eq. 28. Sampling rate = 200 kHz, no. of data points = $2 \cdot 10^6$ with *ca.* 28,000 transitions. Anti-aliasing filter 50 kHz. (*A*) to (*D*): SNR = 25, (*E*) to (*G*): SNR = 1. The mean values (in 1/msec) are the numbers at the abscissa in (*A*) to (*D*). The mean values and the standard deviations σ are also given in Table 2.

The small deviations of the mean values in Table 2 (except row no. 6) indicates that the results can be improved by using longer time series. This is illustrated for the next model.

The performance of the fitting routine also depends on the selected model. The analysis of an ensemble with 2 channels with the configuration (*A* and *O* have equal conductance, rate constants in sec^{-1})

$$\begin{matrix} & k_{OC}=1000 & & k_{AO}=50 & & k_{GA}=400 & \\ C & \leftrightarrows & O & \leftrightarrows & A & \leftrightarrows & G \\ & k_{CO}=500 & & k_{OA}=30 & & k_{AG}=200 & \end{matrix} \qquad (30)$$

did not give satisfactory results even with SNR = 25 (Fig. 7) when time series with $2 \cdot 10^6$ data points are used. Time series with $10 \cdot 10^6$ data points (Fig. 8) gave much better results. This becomes obvious in Table 3

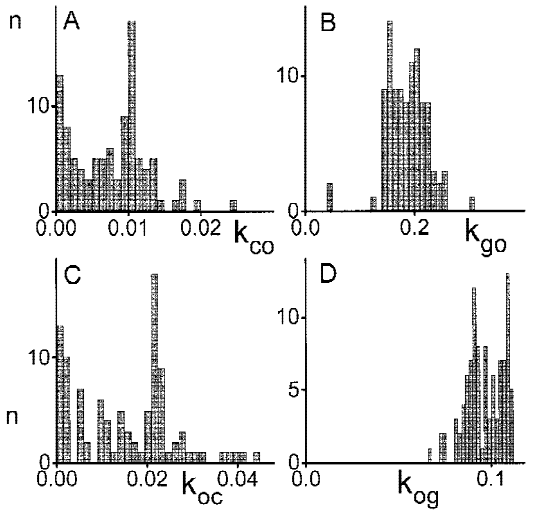

Fig. 5. Histograms of the single-channel rate constants of a *C-O-G* model obtained from 100 simulations of model with 8 identical channels as specified in Eq. 29. The SNR was 1 as in Fig. 4 *E* to *H*. However, in contrast to Fig. 4, the rate constants were divided by a factor of 5. Sampling rate = 200 kHz, no. of simulations = 10^7 with *ca.* 7,000 transitions. Anti-aliasing filter 50 kHz. The mean values (in 1/msec) and the standard deviations σ are given in Table 2.

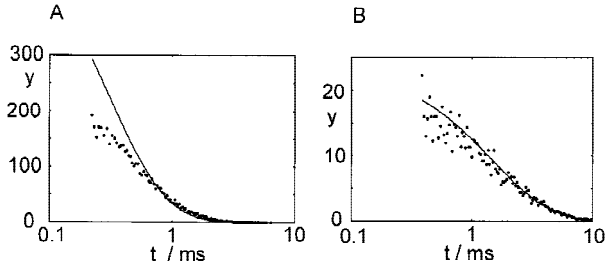

Fig. 6. Failure of the jump detector in noisy 8-channel recordings (SNR = 1) as illustrated by the dwell-time distributions (*see* Fig. 2) of the current level 2 for the *C-O-G* model with (*A*) the rate constants of Fig. 4 (Eq. 28) and (*B*) with the slower rate constants of Fig 5 (Eq. 29). The smooth lines give the ''true'' curve as calculated by means of Eq. 16 using the original rate-constants. The dots are the number of sojourns determined by the Hinkley detector. The situation was similar for the other levels, besides that the number of data points was very low in level 8 and that the discrepancy was much smaller for level 0.

showing the mean values and the standard deviations of the 4-state model fits.

Channel Interaction

In the introduction it was mentioned that a major benefit of the macrochannel in Fig. 1 is the possible introduction of special conditions. One of these is channel interaction. This is demonstrated for a 2-state 4-channels example with the rate constants given in the legend of Fig. 9.

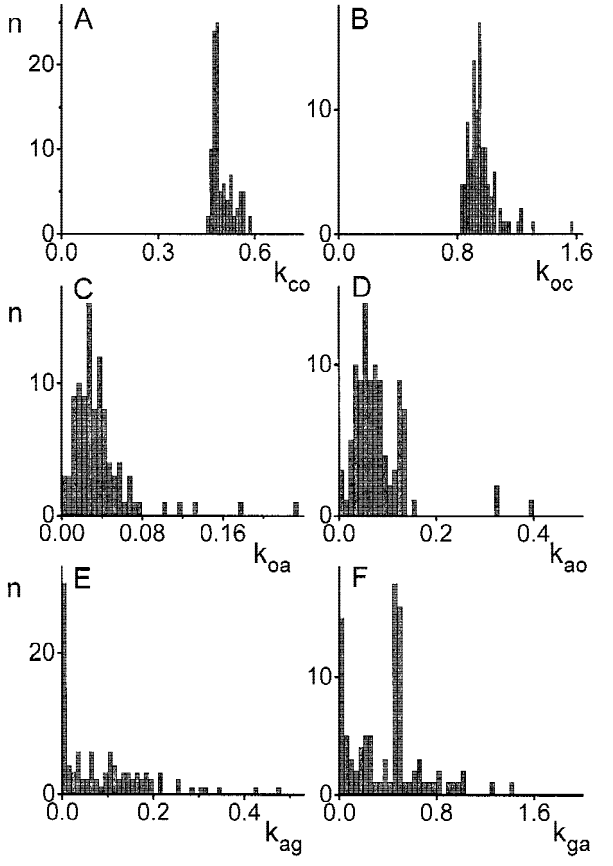

Fig. 7. Histograms of the single-channel rate constants obtained from 100 simulations of model with 2 identical 4-state channels (*C-O-A-G* with O and *A* being open) as specified in Eq. 30. Sampling rate = 200 kHz, no. of data points = $2 \cdot 10^6$ and *ca.* 58,000 transitions. Anti-aliasing filter 50 kHz. SNR = 25. The mean values (in 1/msec) and the standard deviations σ are given in Table 2.

Channel interaction is introduced by making the rate constants of channel opening dependent on the number m of open channels, e.g.

$$k_{ij} = k_{ijO}\,(1 + c \cdot m) \tag{31}$$

for index i belonging to state Y_m and index j to state Y_{m+1} · c is the interaction factor, which increases the open probability if neighboring channels are open. This is an arbitrary example in order to illustrate the method. Iwasa et al. (1986) have found the opposite effect, a decreasing of the opening rate constant when another channel is already open.

With $c = 0.2$, $k_{CO} = 500\ \text{sec}^{-1}$ and $k_{OC} = 2{,}000\ \text{sec}^{-1}$, Eq. 31 leads to the following transition matrix of the *C-O* model (rate constants in 1,000 sec^{-1}).

$$K = \begin{bmatrix} -2 & 2 & 0 & 0 & 0 \\ 2 & -3.8 & 1.8 & 0 & 0 \\ 0 & 4 & -5.4 & 1.4 & 0 \\ 0 & 0 & 6 & -6.8 & 0.8 \\ 0 & 0 & 0 & 8 & -8 \end{bmatrix} \tag{32}$$

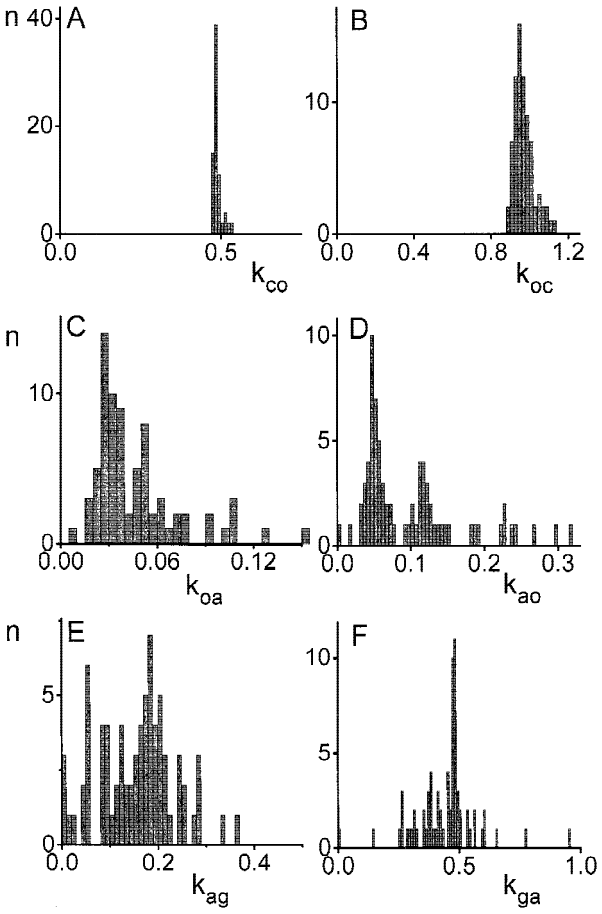

Fig. 8. Histograms of the single-channel rate constants obtained from 100 simulations of a model with 2 identical 4-state channels (*C-O-A-G* with *O* and *A* being open) as specified in Eq. 30. Conditions as in Fig. 7, but 10^7 data points in a time series. The mean values (in 1/msec) of the distributions and the standard deviations σ are given in Table 3.

Eq. 31 introduces channel interaction into the elements above the diagonal in Eq. 32. The rate-constant κ_{12} corresponds to the opening of one channel. As $b_1^{(1)}$ is 4 (each one of the four closed channels can open), its value is 4 k_{CO} = 2,000 sec^{-1} with $m = 0$ in Eq. 31. The strongest effect of channel interaction is found in κ_{45} = 800 sec^{-1}, even though it is the smallest of the opening rate-constants (because $b_1^{(4)} = 1) \cdot b_1^{(4)} k_{CO}$ is increased to $\kappa_{45} = b_1^{(4)} k_{CO} (1 + 3 \cdot 0.2) = 800$ sec^{-1}, because m in Eq. 31 is 3 (three channels open).

To show the convergence of the algorithm *per se*, nearly noise-free simulations were done (SNR = 25). 145 simulated records with $2 \cdot 10^6$ data points were subject to the fitting routine (without visual control). The rate-equations (Eqs. 2, 15 and 16) could be solved by the same software as used for the examples above. However, the calculation of the steady-state concentrations $R_r(\infty)$ required some extra thoughts. Whereas in the case of channel interaction-free models, Eq. 8 could be used, the data with channel interaction required the calculation of the steady-state conditions by using the full matrix equation with $dR/dt = 0$ (Eqs. 2 and 9).

The distribution of the resulting single-channel rate constants and of the channel interaction factor *c* are shown in Fig. 9. The bias of the mean values of the fitted parameters is about 10% in the case of rate constants. The mean value of the channel interaction factor gave the best result with a bias of 0.1%.

We investigated what would happen if the above data simulated with channel interaction were fitted by a channel interaction-free model. For this purpose, the fitting routine was not allowed to use *c* in Eq. 31 ($c = 0$, as in the simulations of the preceding section). Figure 10 shows a comparison of the fits with and without allowing channel interaction. Only the upper three levels are shown, because a deviation was not seen in the levels zero and one channel open. For the level with zero channels open, a deviation would not be expected ($m = 0$ in Eq. 31). In the first level, the effect is still small.

Figure 10 shows that the failure of the model ignoring channel interaction increases with the number of open channels. The deviation is maximum when the fourth channel goes in the open state (Fig. 9*B*).

Figures 9 and 10 demonstrate that the macrochannel approach can be used to test for channel interaction.

Conclusions and Recommendations for Fitting the Data

In the introduction the question was raised whether the results of the simple fit of dwell-time histograms (without corrections for missed events) can be used as final results or whether their role is restricted to that of providing starting values for more sophisticated and more time-consuming approaches. Figures 3 and 9 show good results. In Figs. 4 *A–D*, 5, 7 and 8, at least the faster rate constants around 1,000 sec^{-1} are obtained with reasonable reliability.

However, the simulations also show the flaws of the method. There are the complete failures in Fig. 4 *E–H*, and the broad distributions of the slow rate-constants in other figures. The failures are of different origin. In the case of Fig. 7, the fits could be improved (Fig. 8) by increasing the length of the time series by a factor of 5. This implies that the statistical significance of the time series was not reached, and the application of more sophisticated methods would not help.

On the other hand, the improvement of the fits of Fig. 4 *E–F* by slowing down the rate constants by a factor of 5 (Fig. 5) is an indication that a missed-events correction were necessary. The missed-events problem is also the reason for the influence of noise illustrated by the difference between the upper and lower half of Fig. 4. As the integration time of the Hinkley detector (Schultze

Table 3. Comparison of the mean values (in sec^{-1}) obtained from fitting the 4-state model of Eq. 30 with two channels and different numbers of data points (Figs. 7 and 8)

k_{ij}/sec^{-1}			k_{CO}	σ	k_{OC}	σ	k_{OA}	σ	k_{AO}	σ	k_{AG}	σ	k_{AG}	σ
ch	SNR	MS	1000		500		30		50		200		400	
2	25	2	963	108	499	32	37	33	86	82	90	99	530	1062
2	25	10	972	51	488	14	47	28	98	68	155	79	503	530

ch = numbers of channels, SNR = signal to noise ratio (Eq. 27), MS = 10^6 samples.

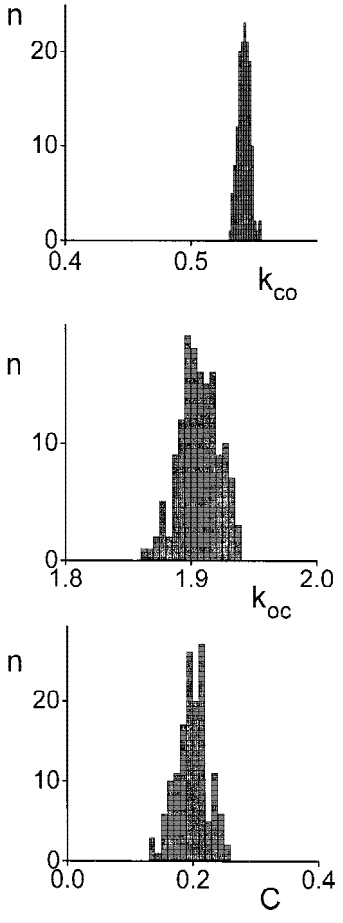

Fig. 9. Histograms of the rate constants and channel interaction factor obtained from 145 simulations of a 2-state (*C-O*) model with 4 channels and with a channel interaction factor of $c = 0.2$ according to Eq. 31. The nominal values were: $k_{CO} = 500$ sec^{-1} kHz, $k_{OC} = 2{,}000$ sec^{-1}. The mean values (in $msec^{-1}$) of the distributions and the standard deviations σ are given in Table 3.

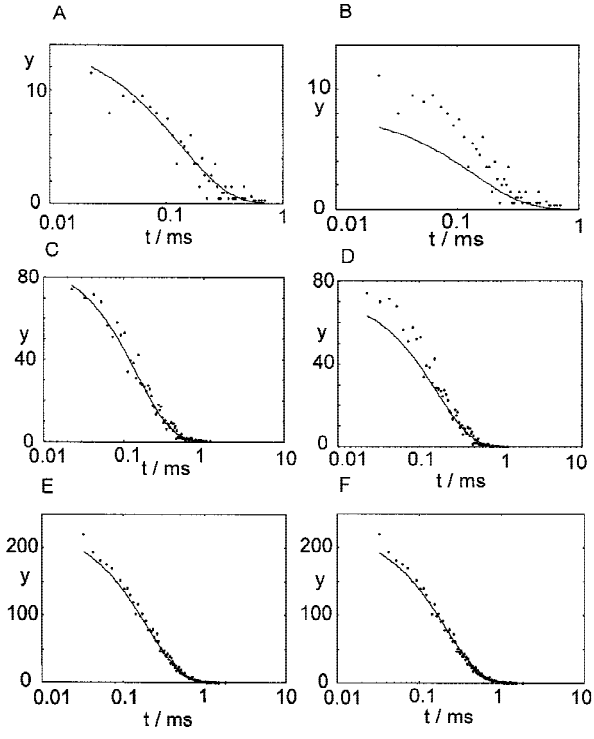

Fig. 10. Comparison of the fits of the dwell-time histograms (*see* Fig. 2) of the channel interaction model of Fig. 9 fitted by a channel interaction model (*A*), (*C*) and (*E*), and by a model without channel interaction (*B*), (*D*) and (*F*). Only the fits of level 4 (*A,B*), level 3 (*C,D*) and level 2 (*E,F*) are shown.

& Draber, 1993) is adjusted to the SNR, the dead time of the detector is much longer in the lower part of Fig. 4. The results here are similar to those of Colquhoun et al. (1996) that the slower time constants suffered more than the medium one from undetected interruptions of long sojourns.

The question may be raised whether the quality of the fits in Figs. 4, 5, 6 and 7 can be improved by using a different fitting strategy. It may be assumed that the bias is a fault of the least square fit (LS) which is known to lead to biased estimates. In a recent investigation we have replaced the least-square fit by a Maximum-Likelihood (ML) estimator. The simulations have shown that there is a better performance of the ML estimator if the time constants are in the middle of the time window (the range given by the anti-aliasing filter and the length of the time series), but LS does better if the time constants are at the edges of the time window. This is just the region where the missed-events problem would come into play.

To test the significance of the error sums, the de-

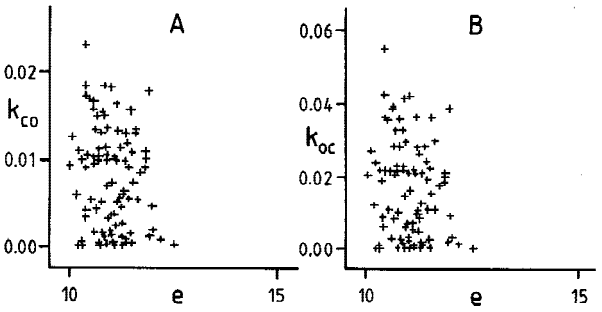

Fig. 11. Relationship between error sum *e* (on the abscissa) and estimated values of the rate constants (in $msec^{-1}$) k_{CO} (*A*) and k_{OC} (*B*) for the simulations of Fig. 5*a* and *C*, respectively.

pendence of the fit quality on the error sums was investigated. The fits of the 8-channel ensemble in Fig. 5 gave really poor results, and thus the fitted values of the k_{ij} were plotted *vs.* the error sum. It was expected that a vertical line presenting an adequate maximum error sum could be drawn which would separate the awful values e.g., of k_{OC} in Fig. 5*A* at 0.0 from those close to 0.1. However, plotting k_{ij} *vs.* the error sum resulted in a rectangular cloud with no visible trend (shown for k_{CO} and k_{OC} in Fig. 11). The interesting finding is that the density distribution of the k_{OC} cloud was found to be surprisingly similar to the k_{CO} cloud (Fig. 11). This indicates that the ratio k_{CO}/k_{OC} does not scatter. This ratio gives the ratio of equilibrium ''concentrations'' of *O* and *C*, which was obviously well determined by the data, but the curve-shape of the dwell-time histogram (related to the temporal behavior) was not.

The problem for the researcher working on real data is that only a handful of data are available and distributions like those shown here can usually not be obtained from the measured data. Thus, the researcher does not know how broad the distributions are, whether the results of the fits are in the tail or in the center of the distribution, and whether there is a bias. However, this information is necessary to determine whether a further analysis with the more sophisticated methods mentioned in the induction is necessary.

Help may come from the methods used for the construction of the distributions as in Fig. 4. It is suggested to take the mean values of the fitted rat-constants, use them for simulations and create distributions like those in Figs. 3, 4, 5, 7, 8 or 9 under the conditions of the experiments (SNR, filter, length). Broad distributions would indicate that the time series are probably too short for a sufficient statistical significance. In that case, also a more sophisticated method would not help. However, double peaks of the fast rate constants (Draber & Schultze, 1994; Magleby & Weiss, 1990*a*) would indicate that the temporal resolution is not good enough, in that case refitting with a better method is recommended. The same holds if a strong bias occurs, i.e., if the center of the distributions does not coincide with the rate constants used for the simulation. The shift of a medium time constant to higher values as caused by missed interruptions (Colquhoun et al., 1996) would be continued in the simulated data, and thus can be detected.

Another way is to take those data sets that provided rate constants that are close to the averaged values of the whole experiment and subject them to one of the more sophisticated approaches mentioned in the introduction. Then it has to be determined whether both approaches lead to the same results.

We are grateful to Mrs. Maike Keunecke and Mr. Dirk Kukulenz for stimulating discussions and to Prof. Dr. O. Pongs, Hamburg, for useful hints.

References

Albertsen, A., Hansen, U.P. 1994. Estimation of kinetic rate constants from multichannel recordings by a direct fit of the time series. *Biophys. J.* **67:**1393–1403

Ball, F., Milne, R.K., Yeo, G.F. 1993. On the exact distribution of observed open times in single ion channel models. *J. Appl. Prob.* **30:**529–537

Ball, F.G., Rice, J.A. 1992. Stochastic models for ion channels: introduction and bibliography. *Math. Biosci.* **112:**189–206

Ball, F.G., Sansom, M.S.P. 1989. Ion channel gating mechanisms: model identification and parameter estimation from single channel recordings. *Proc. Roy. Soc. Lond.* **B236:**383–416

Blatz, A.L., Magleby, K.L. 1986. Correcting single channel data for missed events. *Biophys. J.* **49:**967–980

Blatz, A.L., Magleby, K.L. 1989. Adjacent interval analysis distinguishes among gating mechanisms for the fast chloride channel from rat skeletal muscle. *J. Physiol.* **410:**561–585

Caceci, M.S., W.P. Cacheris 1984. Fitting curves to data — the simplex algorithm is the answer. *BYTE* **5/84:**340–362

Colquhoun, D., Hawkes, A.G. 1977. Relaxation and fluctuations of membrane currents that flow through drug-operated channels. *Proc. R. Soc. Lond.* **B199:**231–262

Colquhoun, D., Hawkes, A.G. 1981. On the stochastic properties of single ion-channels. *Proc. R. Soc. Lond.* **B211:**205–235

Colquhoun, D., Hawkes, A.G. 1982. On the stochastic properties of bursts of single ion-channel openings and of clusters of bursts. *Phil. Trans. R. Soc. Lond.* **B300:**1–59

Colquhoun, D., Hawkes, A.G. 1987. A note on correlations in single ion channel records. *Proc. R. Soc. Lond.* **B230:**15–52

Colquhoun, D., Hawkes, A.G. 1990. Stochastic properties of ion channel openings and bursts in a membrane patch that contains two channels: evidence concerning the number of channels present when a record containing only single openings is observed. *Proc. R. Soc. Lond.* **B240:**453–477

Colquhoun, D., Hawkes, A.G. 1995. The principles of the stochastic interpretation of ion-channel mechanism. *In:* Single Channel Recording. B. Sakmann and E. Neher, editors. pp. 397–482. Plenum Press, NY

Colquhoun, D., Hawkes, A.G., Srodzinski, K. 1996. Joint distributions of apparent open times and shut times of single ion channels and the maximum likelihood fitting of mechanisms. *Phil. Trans. R. Soc. Lond.* **A354:**2555–1290

Colquhoun, D., Sigworth, F.J. 1983. Fitting and statistical analysis of

single channel records. *In:* Single Channel Recording. B. Sakmann and E. Neher, editors. pp. 191–263. Plenum Press, NY

Crouzy, S.C., Sigworth, F.J. 1990. Yet another approach to the dwell-time omission problem of single-channel analysis. *Biophys. J.* **58:**731–743

Draber, S., Hansen, U.P. 1994. Fast single-channel measurements resolve the blocking effect of Cs^+ on the K^+ channel. *Biophys. J.* **67:**120–129

Draber, S., Schultze, R. 1994. Correction for missed events based on a realistic model of a detector. *Biophys. J.* **66:**191–202

Draber, S., Schultze, R., Hansen, U.P. 1993. Cooperative behavior of K^+ channels in the tonoplast of *Chara corallina*. *Biophys. J.* **65:**1553–1559

FitzHugh, R. 1983. Statistical properties of the asymmetric random telegraph signal with application to single channel analysis. *Mathematical Bioscience* **64:**75–89

Fredkin, D.R., Montal, M., Rice J.A. 1985. Identification of aggregated Markovian models: application to the nicotinic acetylcholine receptor. *In:* Proceedings of the Berkely Conference in Honor of Jerzy Neyman and Jack Kiefer. L.M. Le Cam and R.A. Olshen, editors. pp. 269–289 Wadsworth, Monterey

Fredkin, D.R., Rice, J.A., 1992. Maximum likelihood estimation and identification directly from single-channel recordings. *Proc. R. Soc. Lond.* **B249:**125–132

Hansen, U.P., Albertsen, A., Moldaenke, C., Draber, S., Schultze, R. 1995. Detecting events in signals from sensors: the Hinkley-detector is the answer. *Sensors and Materials* **7:**289–300

Hansen, U.P., Keunecke, M., Blunck, R. 1997. Gating and permeation models of plant channels. *J. Exp. Bot.* **48:**365–382

Hawkes, A.G., Jalali, A., Colquhoun, D. 1990. The distribution of the apparent open times and shut times in a single channel record when brief events cannot be detected. *Phil. Trans. R. Soc. Lond.* **A332:**511–538

Hawkes, A.G., Jalali, A., Colquhoun, D. 1992. Asymptotic distributions of apparent open times and shut times in a single channel record allowing for the omission of brief events. *Phil. Trans. R. Soc. Lond.* **A337:**383–404

Horn, R.A., Lange, K. 1983. Estimating kinetic constants from single channel data. *Biophys. J.* **43:**207–223

Iwasa, K., Ehrenstein, G., Moran, N., Jia, M. 1986. Evidence for interactions between batrachtoxin-modified channels hybrid neuroblastoma cells. *Biophys. J.* **50:**531–537

Jackson, M.B. 1997. Inversion of Markov processes to determine rate constants from single-channel data. *Biophys. J.* **73:**1382–1394

Kienker, P. 1989. Equivalence of aggregated Markov models of ion-channel gating. *Proc. Roy. Soc. Lond. Biol.* **236:**269–309

Kijima, S., Kijima, H. 1987*a*. Statistical analysis of channel current from a membrane patch: I. Some stochastic properties of ion channels or molecular systems in equilibrium. *J. Theor. Biol.* **128:**423–434

Kijima, S., Kijima, H. 1987*b*. Statistical analysis of channel current from a membrane patch: II. A stochastic theory of a multi-channel system in the steady-state. *J. Theor. Biol.* **128:**435–455

Kim, E., Niethammer, M., Rothschild, A., Jan, Y.N., Sheng, M. 1995. Clustering of Shaker-type K^+ channels by interaction with a family of membrane-associated guanylate kinase. *Nature* **378:**85–88

Kiss, T., Nagy, K. 1985. Interaction between sodium channels in mouse neuroblastoma cells. *Eur. Biophys. J.* **12:**13–18

Klein, S., Timmer, J., Honerkamp, J. 1997. Analysis of multichannel patch-clamp recordings by Hidden Markov Models. *Biometrics* **53:**870–884

Klieber, H.-G., Gradmann, D. 1993. Enzyme kinetics of the prime K^+ channel in the tonoplast of Chara: selectivity and inhibition. *J. Membrane Biol.* **132:**253–265

Korn, S.J., Horn, R. 1988. Statistical discrimination of fractal and Markov models of single-channel gating. *Biophys. J.* **54:**871–877

Liu, Y., Dilger, J.P. 1993. Application of the one- and two-dimensional Ising models to studies of cooperativity between ion channels. *Biophys. J.* **64:**26–35

Magleby, K.L., Weiss, D.S. 1990*a*. Estimating kinetic parameters for single channels with simulation. A general method that resolves the missed event problem and accounts for noise. *Biophys. J.* **58:**1411–1426

Magleby, K.L., Weiss, D.S. 1990*b*. Identifying kinetic gating mechanisms for ion channels by using two-dimensional distributions of simulated dwell times. *Proc. R. Soc. Lond.* **B241:**220–228

Magleby, K.L., Song, L. 1992. Dependency plots suggest the kinetic structure of ion channels. *Proc. R. Soc. Lond.* **B249:**133–142

Manivannan, K., Ramanan, S.V., Mathias, R.T., Brink, P.R. 1992. Multichannel recordings from membranes which contain gap junctions. *Biophys. J.* **61:**216–227

McGeoch, M.W., McGeoch, J.E.M. 1994. Power spectra and cooperativity of a calcium-regulated cation channel. *Biophys. J.* **66:**161–168

McManus, O.B., Magleby, K.L. 1989. Kinetic time constants independent of previous single channel activity suggest Markov gating for a large conductance Ca-activated K channel. *J. Gen. Physiol.* **94:**1037–1070

Neher, E., Stevens, C.F. 1977. Conductance fluctuations and ionic pores in membranes. *Ann. Rev. Biophysics Bioengineering* **6:**345–381

Press, W.H., Flannery, B.P., Teukolsky, S.A., Vetterling, W.T. 1987. Numerical Recipes. The Art of Scientific Computing. Cambridge Univerity Press, Cambridge, New York, New Rochelle, Melbourne, Sidney

Qin, F., Auerbach, A., Sachs, F. 1996. Estimating single channel kinetic parameters from idealized patch clamp data containing missed events. *Biophys. J.* **70:**264–280

Riessner, T. 1994. Statistische Analyse von schnellen Schaltereignissen in Patch-Clamp Daten mit Hilfe von erweiterten Beta-Verteilungen. Diploma Thesis, Kiel.

Rothberg, B.S., Bello, R.A., Magleby, K.L. 1997. Two-dimensional components and hidden dependencies provide insight into ion channel gating mechanisms. *Biophys. J.* **72:**2524–2544

Roux, B., Sauvé, R. 1985. A general solution to the time interval omission problem applied to single channel analysis. *Biophys. J.* **48:**149–158

Schultze, R., Draber, S. 1993. A nonlinear filter algorithm for detection of jumps in patch-clamp data. *J. Membrane Biol.* **132:**41–52

Sine, S.M., Claudio, T., Sigworth, F.J. 1990. Activation of Torpedo acethylcholine receptors expressed in mouse fibroplasts: single channel current kinetics reveal distinct agonist binding affinities. *J. Gen. Physiol.* **96:**395–437

Song, L., Magleby, K.L. 1994. Testing for microscopic reversibility in the gating of maxi K^+ channels using two-dimensional dwell-time distributions. *Biophys. J.* **67:**91–104

Weiss, D.S., Magleby, K.L. 1989. Gating scheme for single GABA-activated Cl^- channels determined from stability plots, dwell-time

distributions, and adjacent-interval durations. *J. Neuroscience* **9:**1314–1324

Yellen, G. 1984. Ionic permeation and blockade in Ca^{2+} activated K^+ channels of bovine chromaffin cells. *J. Gen. Physiol.* **84:**157–186

Yeo, G.F., Milne, R.K., Edeson, R.O., Madsen, B.W. 1988. Statistical inference from single channel records: two state Markov model with limited time resolution. *Proc. R. Soc. Lond.* **B 235:**63–94

Yeramian, E., Trautman, A., Claverie, P. 1986. Acetylcholine receptors are not functionally independent. *Biophys. J.* **50:**253–263

Appendix I

Steady State Concentrations $R_r(\infty)$ of the Macrochannel

Introducing Eq. 8 into Eq. 7 leads to

$$\frac{d}{dt}R_{r,b^{(r)}} = O = -\left(\sum_{i=1}^{Q} b_i^{(r)} \sum_{\substack{j=1\\ j\neq i}}^{Q} K_{ij}\right)\left(N!\prod_{k=1}^{Q}\frac{(p_{k,\infty})^{(b_k^{(r)})}}{(b_k^{(r)})!}\right) + \sum_{i=1}^{Q}\sum_{\substack{j=1\\ j\neq i}}^{Q}(b_j^{(r)}+1)\,K_{ji}\left(N!\prod_{k=1}^{Q}\frac{p_{k,\infty}{}^{b_k^{(r)}}}{b_k^{(r)}!}\right)\frac{p_{j,\infty}\,b_i^{(r)}}{p_{i,\infty}(b_j^{(r)}+1)} \tag{A1}$$

The last quotient in Eq. A1 accounts for the fact that there is one *j*-state more in R_s than in R_r as given by $b^{(s)} = b^{(r)} + e_j - e_i$ and one less in state *i*.

$$O = \left(N!\prod_{k=1}^{Q}\frac{(p_{k,\infty})^{b_k^{(r)}}}{b_k^{(r)}\,!}\right)\sum_{i=1}^{Q} b_i^{(r)}\left[\sum_{\substack{j=1\\ j\neq 1}}^{Q} -K_{ij} + \sum_{\substack{j=1\\ j\neq 1}}^{Q} k_{ji}\frac{p_{j,\infty}}{p_{i,\infty}}\right] \tag{A2}$$

The last term in Eq. A2 is $\sum k_{ij}$ because of microreversibility $\sum_j k_{ij}\, p_i\,(\infty) = \sum_j k_{ji}\, p_j\,(\infty)$ (Cohquhoun & Hawkes, 1987). Thus, Eq. A2 is zero, and Eq. 8 gives the steady-state solution of Eq. 7.

Appendix 2

Fig. *A*1 shows the block diagram of the program used for the evaluation of the simulated time series.

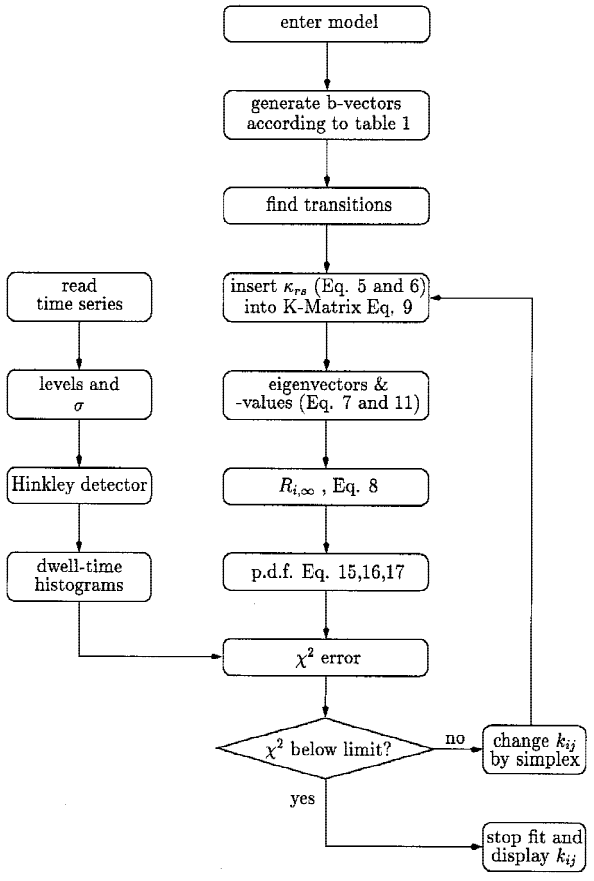

Fig. A1. Block diagram of the fit program; ''levels and σ'': the current-levels and the variance of the noise are determined by two methods: (i) Fit-by-eye: horizontal lines are adjusted in the original time-series, the noise is calculated from the deviations of the data-points. (ii) Amplitude histograms: The levels and the noise are obtained from a simplex-fit of the amplitude histograms with a sum of Gaussian distributions. Level and σ are required by the Hinkley detector to reconstruct the time series. ''enter model'': the number of states, the configuration of the single-channel model, and the number of channels have to be entered. The possible transitions of the single-channel model are communicated to the computer by entering nonzero estimates for the related k_{ij}; ''find transitions'': the single-channel model and the **b**-vectors are inspected in order to find the transitions in the K-matrix; ''χ^2 error'': the error is calculated as (p.d.f – data)^2/ data; ''change k_{ij} by simplex'': A simplex algorithm is employed to find the optimum set of k_{ij}.